Int J Energy Environ Eng (2017) 8:65–80
DOI 10.1007/s40095-015-0183-z

ORIGINAL RESEARCH

Performance of Dish-Stirling CSP system with dislocated engine

Dimitrios Kaliakatsos[1] · Mario Cucumo[1] · Vittorio Ferraro[1] · Marilena Mele[1] · Silvio Cucumo[2] · Alberto Miele[3]

Received: 2 July 2014 / Accepted: 17 June 2015 / Published online: 3 July 2015

Abstract In this paper, a Dish-Stirling Concentrating Solar Power (CSP) system was examined in which the engine works no longer as a receiver but is displaced away from it. In this arrangement it is necessary to adopt a heat transfer fluid capable of transmitting the useful power from the receiver to the hot spring in the Stirling engine head. Various components of the system need designing and especially the heat exchanger in charge of transferring power to the engine head thanks to the cooling of the fluid. The Dish-Stirling system under study includes a linear piston Stirling engine of 4 kW total rated power (3 kW thermal and 1 kW electric). The minimum temperature for starting of the engine is 190 °C, while the maximum is 565 °C. There are many innovative aspects of dish Concentrating Solar Power systems with Stirling engine dislocated, for example, the possibility of using an increased number of engines powered by a single greater dish and energy savings in the solar tracking system. The work covers the search for the most suitable fluids for the purpose, risks and benefit evaluation of fluids never used previously in the field of solar concentration. The heat exchanger sizing was carried out examining different geometric configurations. The study was conducted using a computer and setting up thermo-fluid dynamics simulations in the ANSYS 14.5 environment. Finally, the results were tested and validated through a comparison study with empirical correlations found in the literature.

Keywords Performance · Dish-stirling · CSP system · Dislocated engine

List of symbols

A_f	Cross-sectional area (m^2)
a	Torus section's radius (m)
c	Torus's radius (m)
c_p	Specific heat at constant pressure (kJ kg^{-1} K^{-1})
D_e	Equivalent hydraulic diameter (m)
ΔT	Difference temperature of the fluid among entry and exit (°C)
ΔT_c	Difference temperature among entry fluid and contact surface (°C)
$\varepsilon\%$	Percentage error (%)
f	Darcy's friction coefficient (−)
h	Convective heat transfer coefficient (Wm^{-2} K^{-1})
k	Thermal conductivity (W m^{-1} K^{-1})
$\dot{m}$	Mass flow rate (kg s^{-1})
Nu	Nusselt's number (–)
P_b	Wetted perimeter (m)
P_{cal}	Absorbed power by Stirling engine (W)
P_{el}	Electrical power output produced by Stirling engine (W)
Pe	Peclet's number (–)
P_{max}	Nominal transfer power (W)
P_{pom}	Pumping power (W)
Pr	Prandtl's number (–)

Published in the Special Issue "8th AIGE Conference (Italian Association for Energy Management)".

✉ Dimitrios Kaliakatsos
dimitri@unical.it

Silvio Cucumo
meccanica.cosenza@innova.co.it

Alberto Miele
albertomiele90@gmail.com

[1] DIMEG, University of Calabria, Rende, CS, Italy

[2] INNOVA Solar Energy S.R.L., Via Pedro Alvares Cabrai, 87036 Rende, CS, Italy

[3] Via Monsignor De Angelis, 38, 87010 Terranova da Sibari, CS, Italy

Pr_t Turbulent Prandtl's number (–)
q_W Average power flow (W m^{-2})
Re Reynolds's number (–)
Re_{cr} Critical Reynolds's number (–)
T_b Average fluid's temperature (°C)
T_{eb} Boiling fluid's temperature (°C)
T_{cal} Hot source Stirling temperature (°C)
T_i Entry fluid's temperature (°C)
T_{sa} Setted surface contact temperature (°C)
T_{sc} Calculated surface contact temperature (°C)
T_u Exit fluid's temperature (°C)
T_{sol} Solidification fluid's temperature (°C)
T_w Average temperature of the Transfer surface (°C)
u^+ Wall velocity plus (–)
$\bar{u}$ Undisturbed fluid velocity (m s^{-1})
y^+ Wall y plus (–)
Y Element distance from the wall (m)

Greek symbols

δ Radius of curvature (–)
η Thermal efficiency (–)
μ Dynamic viscosity of the fluid (mPa s)
v Kinematic viscosity of the fluid (m^2 s^{-1})
ρ Fluid's density (kg m^{-3})
τ_w Shear wall stresses (N m^{-2})

Introduction

Solar concentration is one of the most promising technologies in the field of renewable energy supply sources. The increase of solar energy density allows the reduction of absorbing surfaces with resulting cost reduction of individual modules and heat loss reduction related to the size of the latter. Research and development in this area have led to a gradual improvement of the efficiencies and potential use in cogeneration systems through adoption of small-size Stirling engines. Dish-Stirling systems in the market are characterized by a three-dimensional parabolic reflector that concentrates solar radiation in the focus, where the receiver-Stirling engine block is placed.

The high temperatures reached in the focus can be exploited to provide the hot spring of the engine, while cogeneration in Combined Heat and Power (CHP) systems is carried out by removing heat from the cold source using water which can be used for sanitary purposes. Systems of this kind require a two axes movement which ensures the solar trajectory tracking. This work proposes a variant of the classical system, displacing the engine on the ground and inserting a boiler in the focal point of the system. This solution requires a hydraulic circuit and a particular heat exchanger to be mounted on the engine head for heat transfer from the fluid to the motor. The work, through thermo-fluid dynamics simulations performed with ANSYS 14.5, has the aim to select and size the heat exchanger, and the performance evaluation in relation to the heat transfer fluid used.

Bakos and Antoniades [1] performed a study of technical and economic feasibility for a similar system located in Greece.

Dish-Stirling System with dislocated engine

The schematic representation of the proposed system is shown in Fig. 1.

The parabolic reflector and Stirling engine are the same used in the TRINUM system [2], produced and marketed by Innova Solar Energy srl. The receiver, as already said, is made up of a boiler which has the task of transferring power to the thermal transfer fluid. The characteristic curves of the Stirling engine used, manufactured by MICROGEN, are quoted in Fig. 2; Eqs. (1) and (2), experimental type, supplied by the manufacturer, correlate the electrical power produced by the engine and the heat transfer rate absorbed by the same with the contact temperature in correspondence to the hot source.

$$P_{el} = 2.865T_{cal} - 532.5 \quad (1)$$

$$P_{cal} = aT_{cal}^6 + bT_{cal}^5 + cT_{cal}^4 + dT_{cal}^3 + eT_{cal}^2 + fT_{cal} + g \quad (2)$$

Constants of Eq. (2) are reported in Table 1. The manufacturer also provided the values of the temperature limits of engine operation: the minimum temperature for starting being 190 °C, and the maximum temperature of 565 °C, above which engine operation becomes risky.

Thermal transfer fluids

Since the thermal transfer fluid is cyclically subjected to heating inside the receiver and cooling within the heat exchanger, it has to be characterized by high values of conductivity and thermal stability in the range of operating temperatures. Whereas the Stirling engine generates the maximum power at the temperature of 565 °C, the fluid should retain its characteristics up to this threshold value.

The choice of the thermal transfer fluid should not be made only on the basis of its properties, but also considering safety and previous experience gained through its use. Thermal oil is the most cautious choice for safety, even though it manifests too low operating temperatures. The eutectic alloy of sodium and potassium, attractive owing to its low solidification temperature, requires more detailed studies with regard to its dangerousness. Finally,

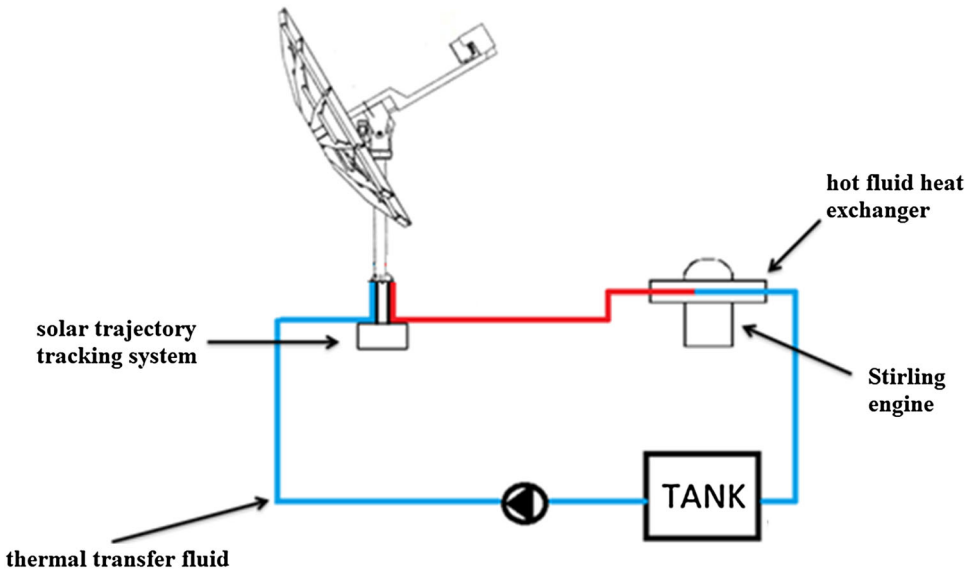

Fig. 1 Scheme of Dish-Stirling system with dislocated engine

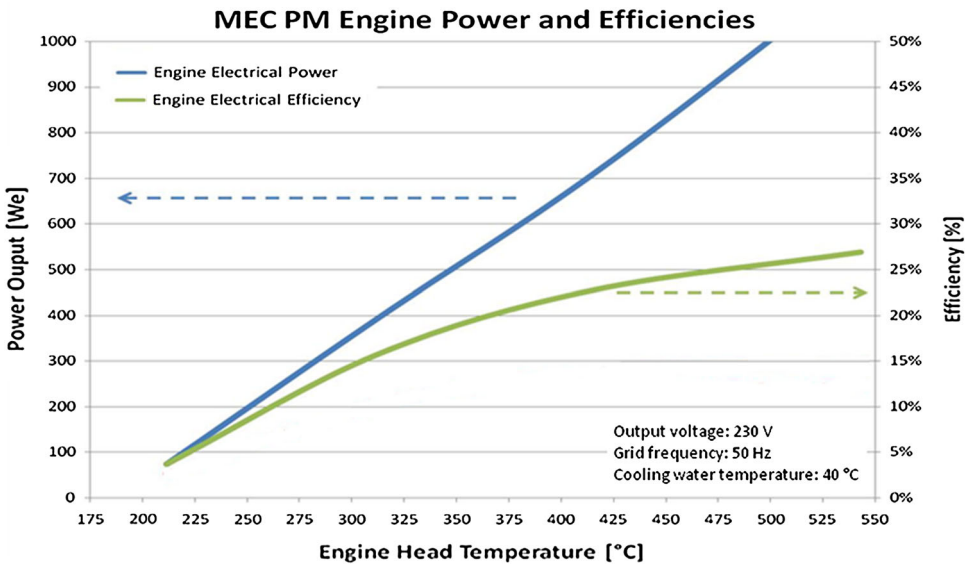

Fig. 2 Characteristic curves of the Stirling engine used

Table 1 Eq. (2) coefficients

a	4.100 E–12
b	−1.085 E–08
c	1.183 E–05
d	6.800 E–03
e	2.193
f	−3.731 E02
g	2.803 E04

air is an alternative to the first two, even though it has inadequate thermal properties and requires definitely higher pumping costs.

The latest generation fluids employ nanotechnology, usable in a thermodynamic solar system. They are being tested by ENEA on the completed SOLAR [3, 4], plant in Puglia. Although they are very promising owing to their thermophysical properties, they require further investigation to verify the safety of nanoparticles on human health.

Diathermic oil

Diathermic oil, much used in Concentrating Solar Power (CSP) systems, can be employed in the liquid phase up to a maximum temperature of 400 °C; in particular Therminol VP-1, eutectic mixture compounded by 73.5 % diphenyl ether and by 26.5 % biphenyl, under the phase change is able to work at the operating temperature of 425 °C.

It starts to burn at temperatures around 120 °C when in contact with air and ignited by a spark. The event could

occur in the case of leakage from the pipes that carry the pressurized fluid from the tank to the heat exchanger.

Maximum engine performance cannot be achieved using this fluid even in the ideal circumstances of unitary heat exchanger efficiency.

Eutectic alloy of sodium and potassium

The latest generation nuclear plants utilize some liquid metals for core cooling that have excellent thermal properties; the use of such fluids in CSP technologies is the subject of discussion in the scientific community [5].

The sodium–potassium eutectic alloy composed of 22.2 % sodium and the remaining part of potassium, unlike solar salts currently used that solidify at a temperature of 230 °C, has a solidification temperature of −12 °C and it can be used up to about 800 °C.

These fluids can react chemically with water, releasing energy (exothermic reaction). Furthermore, in contact with the air, they can burn at temperatures ranging between 130 and 200 °C.

In the case of leakage, the molten sodium, unlike the diathermic oil, solidifies in contact with the atmosphere at ambient temperature and burns into flame individually. The energy released by the combustion, however, is four times lower than diesel combustion and comparable to wood combustion.

The use of such fluids would allow the engine to operate in conditions of maximum power.

Air

It is, clearly, a zero cost fluid, which presents the thermophysical properties that involve significantly lower system performance, at equal flow rates, compared to the use of the fluids illustrated above. To transfer the same power, owing to its low thermal capacity, substantial temperature differences are required. Nevertheless, the employment of this fluid does not involve special measures in relation to safety.

While the thermal oil and the liquid metals have negligible variations of thermophysical properties with temperature, this is not valid for air also because of the high thermal gradients it undergoes in the heat exchanger.

Table 2 shows the thermophysical properties of the three fluids.

Hot fluid heat exchanger

The heat exchanger is inserted in the hot fluid Dish-Stirling system as the last element that transfers power to the Stirling machine. It has the task of moving energy from the hot fluid to the hot walls of the Stirling engine head in the zone of contact with the hot source. The hot fluid will cool in it from the entry conditions to the unknown exit conditions. The component was sized in the research work to ensure the natural connection with engine head.

Figure 3 shows the geometric characteristics of the engine, the red section represents the area in which the engine has to interact with the hot source (heat exchanger). The heat exchanger has a toroidal geometry with a rectangular base. This is a specific shape that ensures a greater heat exchange surface between fluid and solid. Particular attention was paid to the heat exchanger design to avoid contact with the Stirling cold source (shown in blue in Fig. 3).

Circular fins were also inserted inside the heat exchanger with the purpose of increasing the heat exchange surface and facilitating the development of turbulence that can determine greater convective heat transfer coefficients, especially in the case of using a compressible fluid.

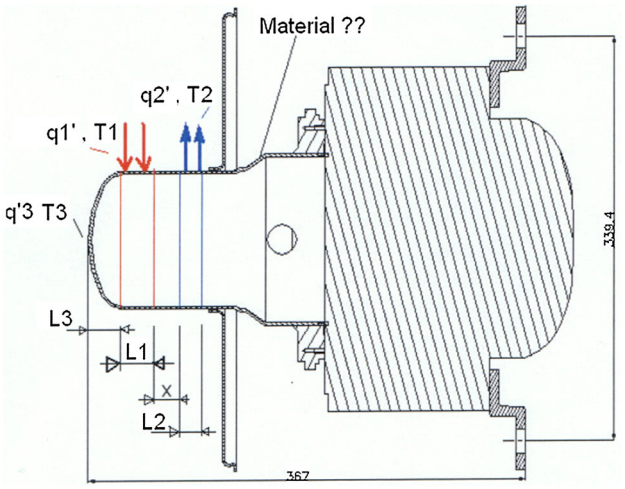

Fig. 3 Scheme of the head of the Stirling engine

Table 2 Thermophysical properties of the three thermal transfer fluids

Fluid	T_{sol} (°C)	T_{eb} (°C)	c_p (kJ kg^{-1} K^{-1})	k (W m^{-1} K^{-1})	ρ (kg m^{-3})	μ (mPa s)
Therminol VP-1	–	400	2.62	0.0759	696	0.147
Eutectic NAK	−12	785	0.87	26.2	750	0.18
Air 728 °C	–	–	1.14	0.068	0.353	0.042
Air 478 °C	–	–	1.09	0.055	0.47	0.035

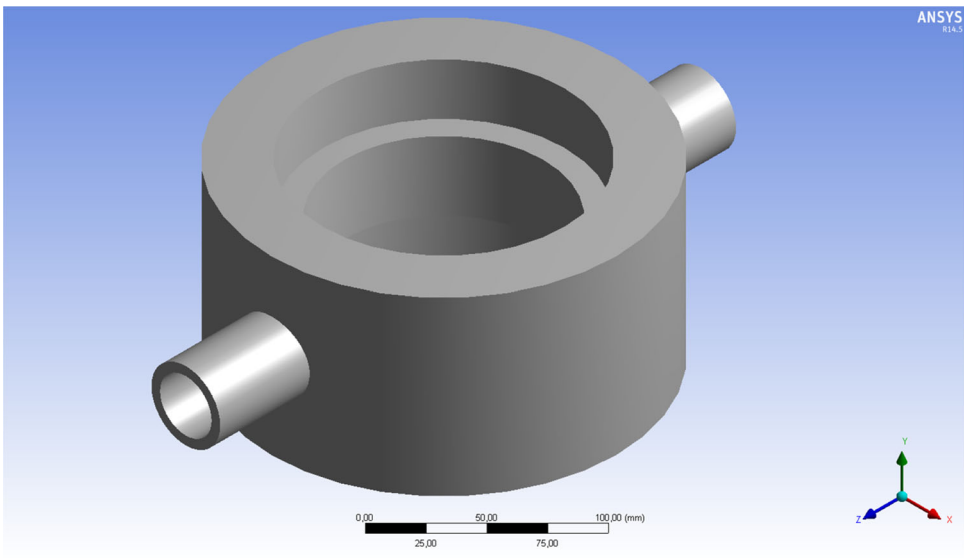

Fig. 4 CAD scheme of heat exchanger

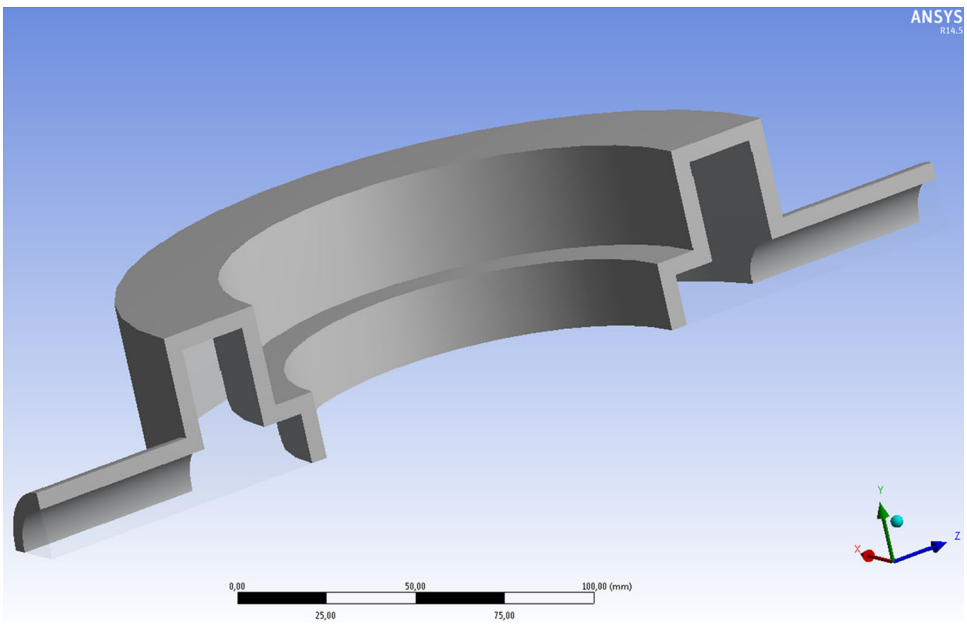

Fig. 5 Computational domain of the configuration 1

The design of the heat exchanger concerned both the fluid used and performance resulting from its combination with the Stirling engine described above.

Figure 4 is the axonometric CAD proposed for the exchanger, in which the supply and outlet ducts of the fluid are visible.

The proposed *Configuration 1*, see Fig. 5, is fundamental for those that follows. In fact, in the successive configurations an increasing number of circular fins with rectangular profile, longitudinal with respect to the fluid flow, were introduced. The fins are connected to the central segment of the heat exchanger. In the figure, we illustrate the solid area in grey and the fluid zone in transparent grey.

Configuration 2 is geometrically different from the first due to the addition of two fins inside the heat exchanger. The fins have a thickness of 4.5 mm and a length of 25 mm. The space between a fin and another is 7 mm. Geometry with these dimensions ensures symmetry with respect to the y–z and x–z planes. In fact, the computational domain includes a single fin, as shown in Fig. 6.

Configuration 3 has three longitudinal fins. The size of the fins and the space between them were modified to ensure symmetry with respect to the usual *x–z* and *y–z* planes. In this configuration, the thickness of the fins is 2 mm while the distance is 6 mm. The other dimensions, including the length of the fins, were unchanged.

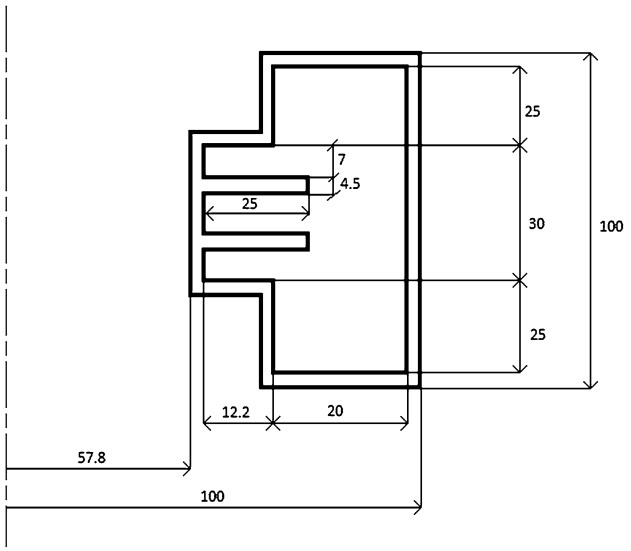

Fig. 6 Passage section of configuration 2

Into *Configuration 4* five longitudinal fins of the same size were inserted, equal to the previous geometries. The increased number of fins resulted in a reduction of the space between fins. In these areas, laminar flow conditions occur that lower the convective coefficients.

Configuration 5 is different from all the others. Starting from configuration 1, transverse fins were added with respect to the fluid flow. The average motion of the heat transfer fluid, in this case, is varied, with the creation of large vortices in the spaces between the fins. These vortices absorb energy from the fluid without really strengthening the heat exchange. In this case there is no turbulence increase but a strong gradient of the average velocity, with consequent reduction of the convective coefficients. A configuration of this kind was discarded in principle not only due to the creation of unwanted large size vortices, but also to the objective difficulty of creating a robust calculation grid for CFD simulation because of the complex geometry. A further problem is the inability to define a hydraulic equivalent diameter because of the unique passage section. Indeed, see Fig. 7, the fluid passage section expands in the zones where the transverse fins are not present, while it narrows in the zones where the transverse fin is present.

Thermo-fluid dynamics analysis

The thermo-fluid dynamics studies involved all the configurations previously proposed. Operating in this manner, it was possible to establish the configuration with greater efficiency. In the implementation phase CFD analysis, it was estimated that configuration 4 ensures the highest heat transfer coefficients. So, a comparison between the three heat transfer fluids proposed was carried out only for this configuration. This involved three studies with different fluid dynamics boundary conditions for the same configuration. Table 3, in which there are geometric relevant numbers, shows configuration 5 that required two different transit sections to be defined (5s for the section without fins and 5c for the section with fins). On the other hand, for configuration 4, naturally the geometric dimensions remain the same even if varies the fluid flowing inside the heat exchanger.

To establish the characteristics of the flow inside the heat exchanger, correlations were sought to define the critical Reynolds number [6] and the friction coefficient. Ito [7], proposes an empirical relationship for flow in circular ducts, see Fig. 8.

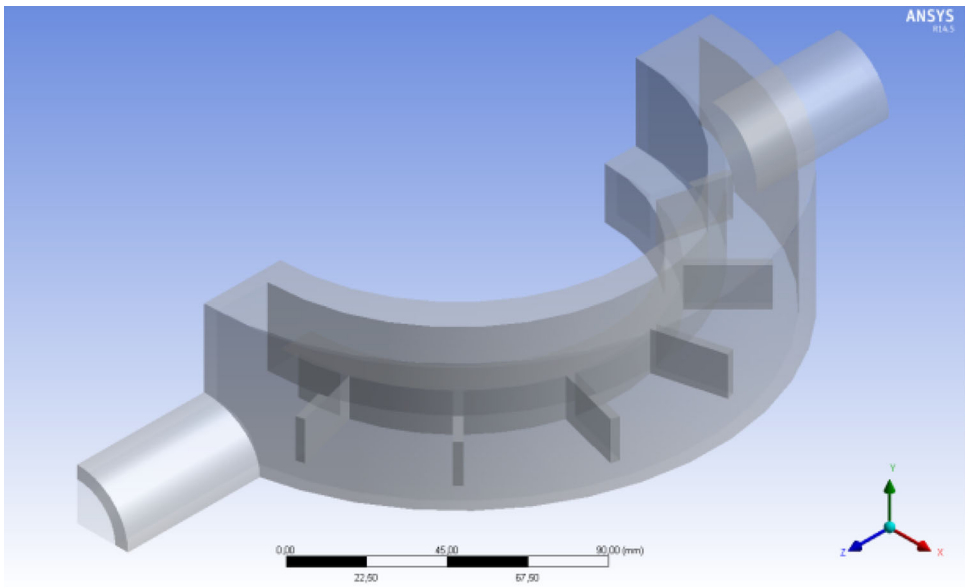

Fig. 7 Computational domain of configuration 5

Table 3 Geometrical size and mass flow rate

	A_f (m^2)	P_b (m)	D_e (m)	δ (–)	$\dot{m}$ (kg s^{-1})
1 (NaK)	21.66	0.234	0.037	0.24	0.53
2 (NaK)	19.41	0.334	0.023	0.15	0.53
3 (NaK)	20.16	0.384	0.021	0.14	0.53
4 (NaK)	19.16	0.484	0.016	0.10	0.53
4 (Air 728 °C)	19.16	0.484	0.016	0.10	0.013
4 (Air 478 °C)	19.16	0.484	0.016	0.10	0.013
4 (Oil)	19.16	0.484	0.016	0.10	0.49
5s (NaK)	21.66	0.234	0.037	0.24	0.53
5c (NaK)	14.16	0.226	0.025	0.16	0.53

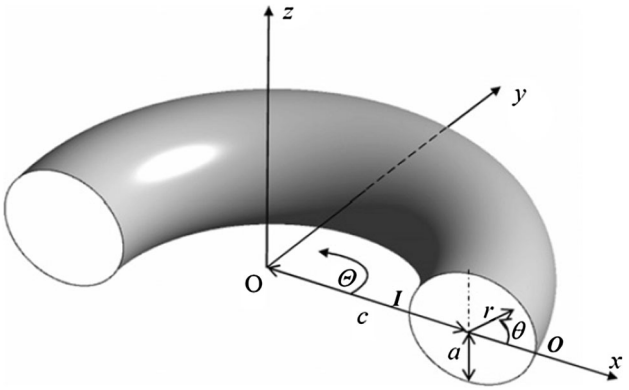

Fig. 8 Circular duct

Table 4 Thermo-fluid dynamics numbers

	Re (–)	Re_{cr} (–)	Pr (–)	Pe (–)
1 (NaK)	15,4167	14302	0.006	925
2 (NaK)	95,833	11721	0.006	575
3 (NaK)	87,500	11293	0.006	525
4 (NaK)	67,000	10124	0.006	402
4 (Air 728 °C)	6724	10124	0.702	4720
4 (Air 478 °C)	10,724	10124	0.702	7528
4 (Oil)	74,154	10124	5.074	376,257
5s (NaK)	154,167	14302	0.006	925
5c (NaK)	104,167	12130	0.006	625

$$f = 0.304 \times \mathrm{Re}^{-0.25} + 0.029\sqrt{\delta} \quad (3)$$

$$\mathrm{Re}_{cr} = 2.1 \times 10^3 (1 + 12\sqrt{\delta}) \quad (4)$$

The relation (3) is useful for the calculation of the Darcy friction coefficient, while (4) allows the calculation of the critical Reynolds (Table 4) in relation to the equivalent hydraulic diameter (Table 3). The term δ [8] is defined as the ratio between the duct radius and the curvature radius of the same. Figure 8 is illustrative of this definition.

$$\delta = \frac{a}{c} \quad (5)$$

Additional thermo-fluid dynamics numbers refer to the individual fluid flow studies accomplished, are reported in Table 4. All values are referred to the cross section of the heat exchanger. It is noted that the simulation with air required an analysis over the entire operation range. It was, therefore, necessary to define the numbers at the extremes of this range (between 478 and 728 °C). It is evident that the flow is turbulent for all the CFD analyses set up, except for the air. In the latter case, in fact, the Re_{cr} number is greater than Re number. Another factor, not to be underestimated, is the characteristic low molecular Prandtl number for liquid metals flows.

The thermo-fluid study of the heat exchanger in question was conducted through fluid dynamics computer simulations (CFD). A model was adopted that reproduced the heat transfer within the fluid and heat transfer throughout the solid parts. A model was adopted to treat the turbulence, given the high values of Reynolds number achieved in the passage section.

The two-equation "*k*-ε" model with special treatment for the on the wall flows, "enhanced wall treatment", was set up in the Fluent environment by means of the ANSYS platform.

The simulations were conducted on calculation grids with a variable number of elements. Indeed, there was some difficulty in dealing with very complex internal geometries, consequently "regular" configurations were chosen. Complications related to the internal geometry are due to the difficulty in creating an acceptable computational grid with the automatic methods such as those used. Each simulation required checking results in a "retroactive" way. The controlled variables are the contact surface temperature and the wall y^+. The former should fall in a neighbourhood of the contact temperature sets during the setup stage to provide the power absorbed by the engine, as shown by Eq. (2). The second control variable is indispensable to verify the validity of the wall turbulence model adopted. A large number of simulations were lost because they had no validity. Owing to the slowness of the fluid dynamics study, the heat exchanger configuration with the highest performance was first examined through qualitative analysis. In a second step, these configurations were examined in depth, creating more elaborate grids and obtaining the convergence of the solutions with more burdensome processes.

CFD analysis

CFD analysis was set up in the Fluent environment through the ANSYS platform. The simulations involved a model

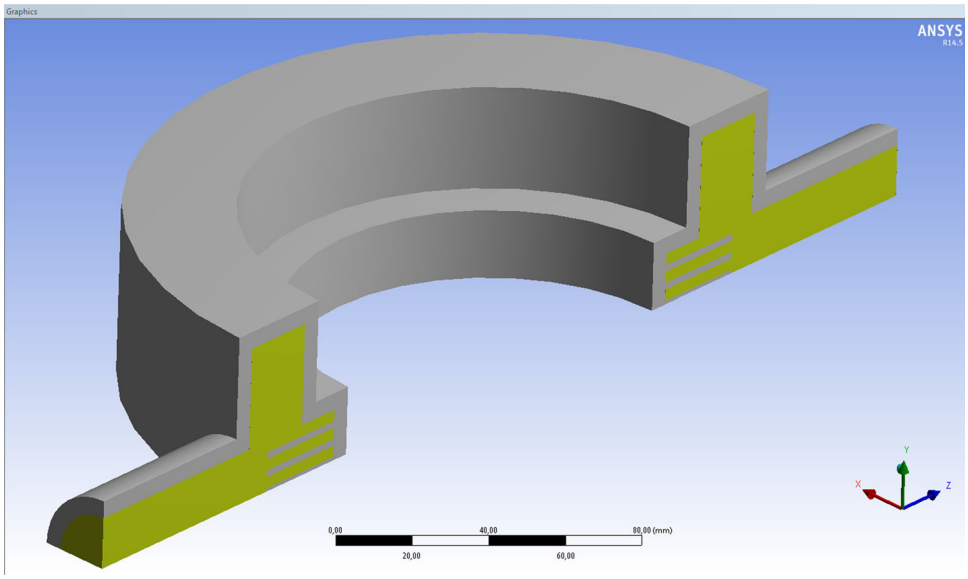

Fig. 9 Computational domain configuration 4

that includes a fluid part and a solid part. Figure 9 shows the simplification of the computational domain to a quarter of the whole, thanks to the symmetries with x–z and y–z planes. The grey part is the solid while the green part is the fluid. Simulations were carried out in steady-state condition through a *pressure-based* solver, SIMPLE scheme; the equations of transport were solved separately.

For all transport equations a *second-order upwind* scheme was chosen for the spatial discretization of the solution.

Turbulence model and wall flow

Turbulence was treated with two additional equations, k–ε model. This model is based on two additional equations for transporting turbulent kinetic energy k, and the transport of the turbulent dissipation ε.

The CFD theory [9] defines three areas for the flow of a fluid in the wall proximity. In this regard, we introduce two dimensionless characteristic quantities, useful for understanding relationships that exist between the velocity and wall distance.

$$y^+ = \frac{y\sqrt{\frac{\tau_w}{\rho}}}{v}; \quad u^+ = \frac{\bar{u}}{\sqrt{\frac{\tau_w}{\rho}}} \tag{6}$$

The wall shear stress (τ_w), the undisturbed fluid velocity ($\bar{u}$) and the distance of the element from the wall (y) appear in these relations. The area in direct contact with the wall is called "under-viscous layer", while moving away from the wall there is the "log-layer" area, as defined owing to the logarithmic relationship that binds y^+ and u^+. Between these two, there is a transition zone, named in the literature as "buffer-layer".

Experimental surveys have shown that the "k–ε" model is not suitable for the treatment of the flow in the under-viscous layer. In this area we use a turbulence treatment model with a single equation following the study proposed by Wolfenstein [10]. The theory exposed by Wolfenstein is valid only in the under-viscous layer and, therefore, for $y^+ \leq 4$.

CFD grids

The specific curvilinear geometry of the heat exchanger in question has resulted in the adoption of a mixed calculation grid, with a few "body-fitted"-type triangular elements. The grids of the different configurations range in size from 1×10^6 to 5×10^6 elements.

The quality of the computing grid was verified by statistical automatically analysis. We proceeded with two verification methods, controlling both the parameter "Aspect Ratio" and the parameter of "Element Quality". The first is defined as the ratio between the longer edge and the shorter edge of the elements. Its optimum value differs according to the type of element analysed: for the rectangular elements the optimal value is one, whereas, for the triangular elements, it is greater than one. The parameter "Element Quality" is the ratio between the volume element and the sum of the lengths of each edge of the same. The optimal value of this parameter is one, but appreciable values greater than 10^{-1} are considered. The aspect ratio is less than 100 for 95 % of the elements and an element quality between 0.8 and 1 for 80 % of the elements in all the grids used for the simulations.

The grids were constructed to achieve a sufficient intensification on the wall, ensuring a y^+ less than 4 and a

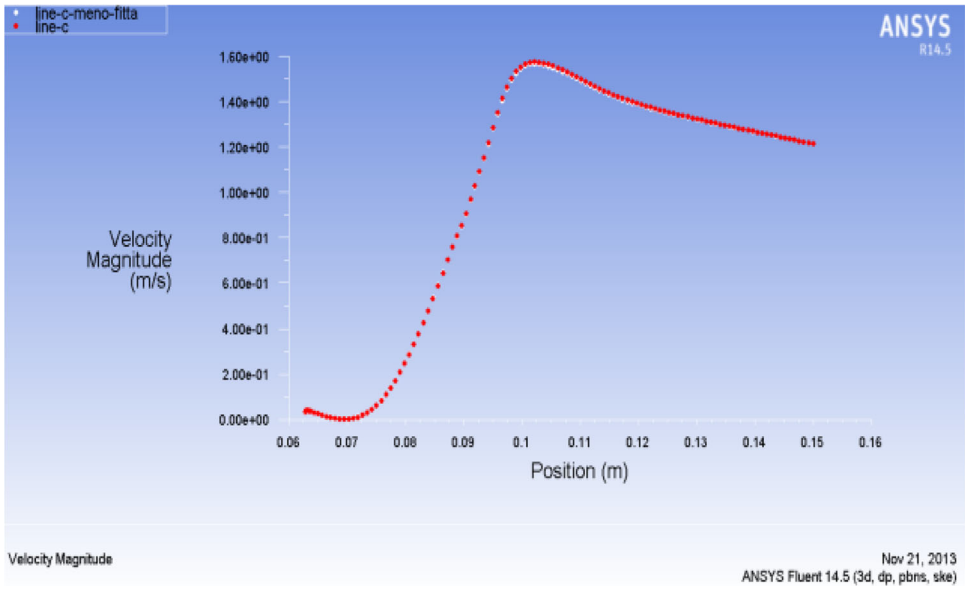

Fig. 10 Velocity magnitude for two different grids, simulation 4 (NaK)

more precise solution in the area where the velocity gradients are the highest.

The independence of the solution from the calculation grid, compatibly with the available calculation means, was demonstrated. The fluid velocity magnitude is the control variable chosen to compare the results of grids of different sizes. The analysis of independence was performed in the areas where the velocity gradients are greater: between the interspace of two fins and in proximity to the solid surface. The comparison was carried out visually, by superimposing the velocity graphs for the two simulations with different calculation grids and, analytically, by calculating the maximum error with the automatic algorithm written in Matlab. Figure 10 shows the trend of the velocity in the interspace between two fins for simulation 4 (NaK), for the grid of 2.57×10^6 elements (white) and for the grid of 4.14×10^6 elements (red).

The percentage deviation, calculated analytically, turns out to be less than 1 % for all tests conducted.

Implementation of the simulations

The implementation of the simulation was carried out by creating two complementary solids during the CAD drawing phase, which were configured with specific properties during the setting of the simulations in Fluent. The solid is compound with copper, whose properties are reported in the database provided by the software. This material was chosen

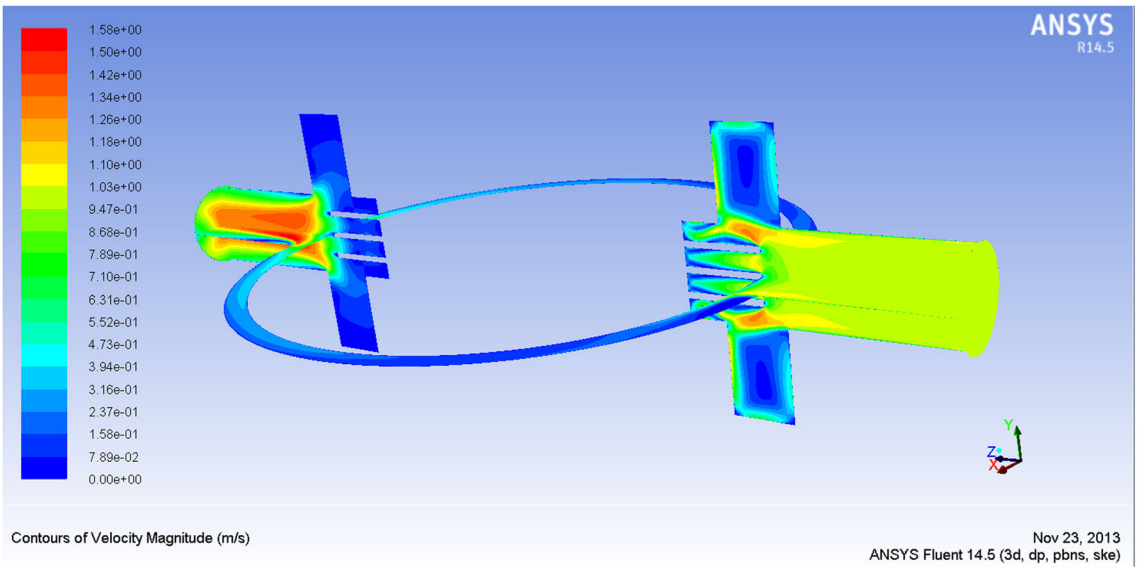

Fig. 11 Velocity magnitude for x–z and y–z planes, simulation 4 (NaK)

because of its excellent quality as a heat conductor and because of its good mechanical and chemical resistance to corrosive fluids. The fluid was defined each time and its properties were imported manually.

Solid modelling in simulations with heat transfer solid/fluid was found from the Fluent theory manual [11] present to support the application. The single equation of energy conservation was solved for these bodies.

Figure 11 shows the trend of the velocity magnitude for the simulation 4 (NaK). The results refer to the symmetry planes x–z and y–z. In the area where there is a sudden narrowing of the section there is a considerable increase of vortices and this is highlighted by the CFD simulations.

Figure 12 shows the temperature of the fluid within the heat exchanger for the simulation 4 (NaK). The area in red is, clearly, the input at high temperature, while that in orange is the output section at a lower temperature. The temperature drop between the two sections is 9.7 °C.

The temperature trend for the solid part is shown in Fig. 13. The temperature decreases passing from the inlet section to the outlet.

Boundary condition

The problem in question is characterized by different boundary conditions.

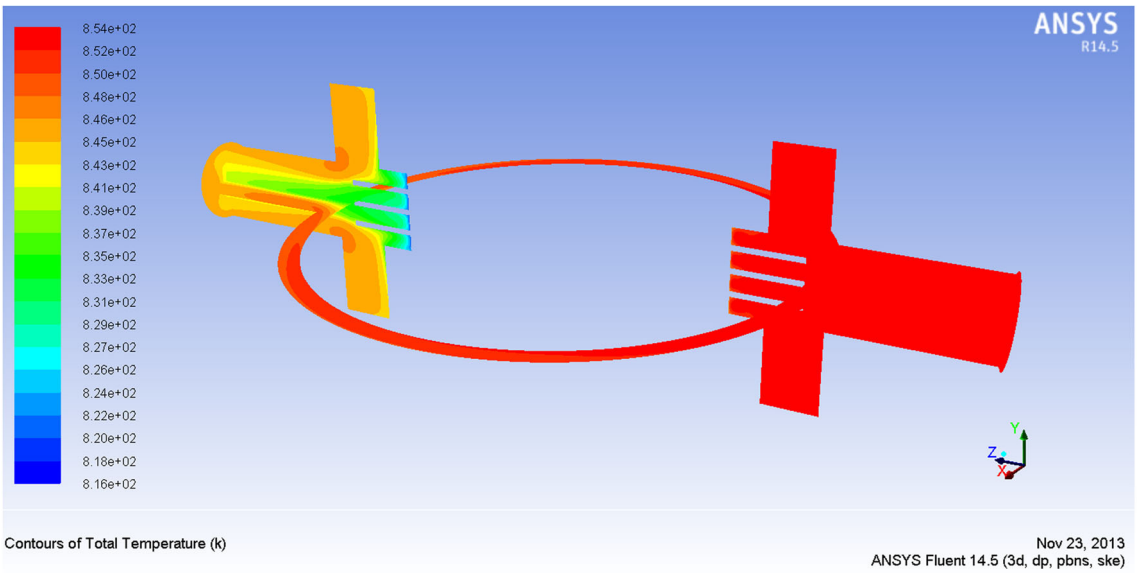

Fig. 12 Temperature for the fluid part for the x–z and y–z planes, simulation 4 (NaK)

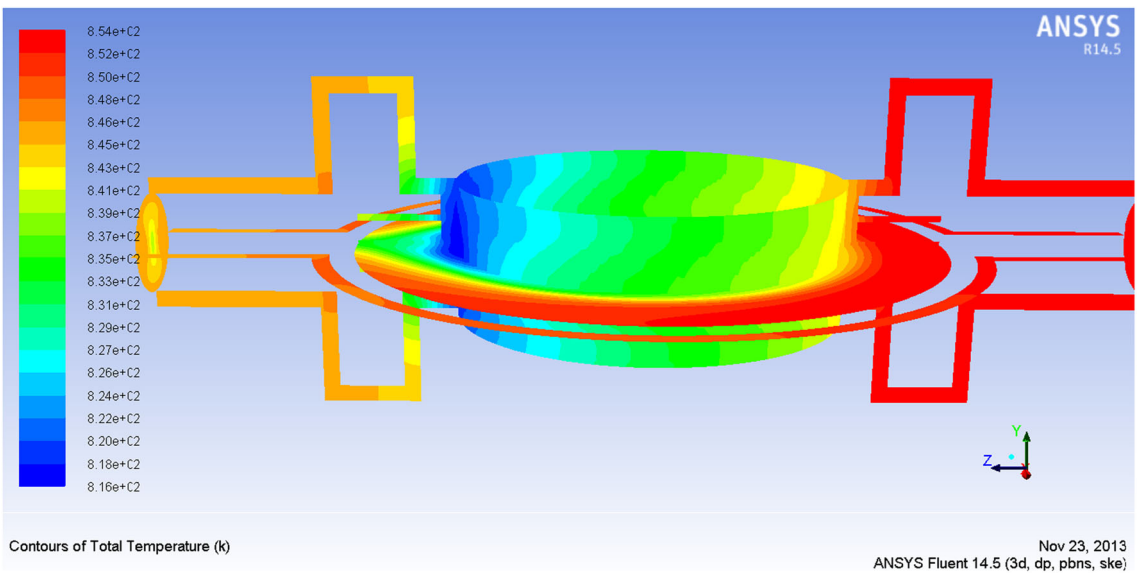

Fig. 13 Temperature for the solid part for the x–z and y–z planes, simulation 4 (NaK)

Inlet section: in the entrance section to the duct that carries the fluid to the heat exchanger, "velocity inlet" condition was imposed. In this boundary condition, an initial value of the turbulence field was assigned, entering a turbulence intensity of 5 % and a ratio of turbulent intensity of 10 [12, 13].

Outlet section: the output section of the end duct of the heat exchanger was configured with the "pressure-based" condition. The pressure imposed for all simulations is zero.

Walls: the "wall" boundary condition was set for all surfaces, which were assumed adiabatic, excluding the inner surfaces of the heat exchanger and the surface of contact with the head of the Stirling engine. A pair of conditions can be imposed for the contact surfaces of the solid–fluid: one called the "shadow" of the other, belonging, respectively, to the fluid and to the solid. Finally, for the contact surface with the head of the engine, as a condition of "wall", a negative power, or absorbed by the engine, in accordance with Eq. (2) was assigned. In Fluent code, the boundary wall condition indicates that the surfaces of the heat exchanger in contact with the engine, exchange a heat transfer rate evaluated by the Eq. (2). This power depends on the variable surface temperature, and the hypothesis considered is not that of constant flow.

Analysis of the results

The in-depth thermo-fluid dynamics study required a reinterpretation of the results for a comprehensive comparison. The different geometric morphologies of the heat exchanger under consideration are venues of discrepant flows between them and they deserve a thorough investigation for the validation of the results. The large vortices observed in the velocity module trend, provide guidance on the turbulent and chaotic motion that is generated inside the heat exchanger. Turbulence is a dissipative phenomenon, so complicated to study that the analyses of fluid flow by computer are carried out through approximate models. Although this method of turbulent CFD analysis is one of the most used, owing to its particular flexibility and "lightness" in terms of the calculation commitment, it introduces numerical errors.

Clearly, the fluid dynamics analysis of the heat exchanger in question is aimed to obtain the most efficient configuration from the thermal point of view, which cannot be separated from the fluid flow inside it. Nevertheless, the validation of the results was carried out by analysing the thermal values, since the objective of the study is focused on these quantities and not on a perfectly resolved turbulent flow. The examined value is the heat exchange convective coefficient on the wall. The latter is obtainable by various empirical correlations proposed in the scientific literature. Therefore, a comparison between the values provided by the empirical correlations and the CFD results was carried out.

The convective coefficient was extrapolated from the CFD results through an indirect calculation. The best configuration among those analysed was traced through a comprehensive comparison. In this phase efficiency was introduced useful to classify the configurations.

Empiric correlation researched

By means of a thorough literature search some correlations considered applicable to the problem were selected.

The first correlation, presented by Roger and Mayhev [14], derived from the most famous Dittus and Boelter's equation which, for fluid cooled, for $\mathrm{Re} > 10^4$ and $0.7 < \mathrm{Pr} < 160$, takes the form:

$$\mathrm{Nu} = 0.023 \times \mathrm{Re}^{0.85} \times \mathrm{Pr}^{0.3} \times \delta^{0.1} \tag{7}$$

Xin and Ebadian [15] presented an experimental study on heat transfer for helical tubes. The correlation proposed by them, which is valid for both air and water, with $0.7 < \mathrm{Pr} < 5$ and Reynolds between 5.5×10^3 and 1.1×10^5 and cooled fluid, is:

$$\mathrm{Nu} = 0.00619 \times \mathrm{Re}^{0.92} \times \mathrm{Pr}^{0.3} \times (1 + 3.455\delta) \tag{8}$$

The investigation on the turbulent heat transfer for eutectic alloys of lead and bismuth, conducted by Cheng and Tak [16] refers to an in-depth study about modelling of the turbulent Prandtl number [17–20] necessary to fully understand these flows. The significance in defining this value is detectable early in the direct influence it exerts in flows with turbulent heat exchange. The definition of $\mathrm{Pr_t}$ is not easy work because of the strong dependence of the turbulent properties on the nature of the motion. The first, in fact, can also change from point to point. The same authors suggest treating the turbulent Prandtl number through empirical models relation and to be wary of automatic calculation models because they are still unreliable. In the CFD simulations, a $\mathrm{Pr_t}$ of 0.85, the default value in FLUENT was used. Lyon [21] proposed a semi-empirical elaboration of a Martinelli's work [22], based on the analogy theory to the turbulence moment and energy transfer.

This work led to the formulation of Nusselt number for heat transfer involving liquid metals:

$$\mathrm{Nu} = 7.0 + 0.025\left(\frac{\mathrm{Pe}}{\mathrm{Pr_t}}\right)^{0.8} \tag{9}$$

Skupinsky et al. [23] conducted studies on other liquid metals of particular thermo-technical interest for heat exchangers. The experiments, performed with a sodium

and potassium fluid, led to the formulation of the following correlation:

$$\mathrm{Nu} = 4.82 + 0.0185 \times \mathrm{Pe}^{0.827} \quad (10)$$

Sleicher [24] performed several experimental investigations on the local heat transfer coefficients for NaK flows in ducts with different boundary conditions. The author concluded that, in the case of uniform wall temperature, the heat transfer coefficients are lower than in the case of uniform heat flux:

$$\mathrm{Nu} = 6.3 + 0.0167 \times \mathrm{Pe}^{0.85} \times \mathrm{Pr}^{0.08} \quad (11)$$

Cheng and Tak, in their research work through CFD simulations for heat transfer of the lead and bismuth eutectic alloys, found results in agreement with those expected from Kirillov's correlation [25] for low Peclet numbers, and with those provided by Stromquist's correlation [26] for high Peclet numbers. The correlation drawn from them is the following:

$$\mathrm{Nu} = A + 0.018 \times \mathrm{Pe}^{0.8}$$

$$A = \begin{cases} 4.5 & \mathrm{Pe} < 1000 \\ 5.4 - 9 \times 10^{-4}\mathrm{Pe} & 1000 < \mathrm{Pe} < 2000 \\ 3.6 & \mathrm{Pe} > 2000 \end{cases} \quad (12)$$

As pointed out by Cheng and Tak, the definition of the turbulent Prandtl number is of paramount importance to conduct flow simulations with liquid metals.

The studies of Cheng and Tak were dedicated to strong flows of liquid metals which is the lead and bismuth eutectic alloy. The latter, although of the same type as the sodium and potassium eutectic alloy, cannot be fully assimilated to the heat transfer fluid considered in this work.

Comparison with empirical correlations

The fluid dynamic simulations on the computer solve the flow field, the pressure field and the temperature of the entire computational domain in relation to the given boundary conditions. Therefore, it is necessary to derive the convective coefficients through an a posteriori calculation of the simulations performed. As the authors Di Liberto and Ciofalo suggest in their work about numerical analysis of turbulent flows in curved pipes [8], the Nusselt number is obtained as a function of the average outgoing or incoming power flow across the exchange surface (q_w), as a function of average temperature of the same surface (T_w) and the average temperature of the entire fluid volume (T_b).

$$\mathrm{Nu} = \frac{q_w \times D_e}{k \times (T_w - T_b)} \quad (13)$$

The heat flow refers to the exchange surface between the solid body and the fluid body. The latter is not equivalent to the contact surface with the engine head. The temperature of the surface, instead, is an average weighted on the exchange area while the temperature of "bulk" is mediated on the fluid volume.

The convective heat transfer coefficient is defined as:

$$h = \frac{q_w}{(T_w - T_b)} \quad (14)$$

Table 5 shows the results of CFD simulations with the calculation of convective coefficients. The approximation of this simulation is remarkable because of the dependence of h from the values of the temperatures; these values are average and not exact values.

The probability, therefore, of finding significant differences with the empirical correlations is very high.

Table 5 shows the values of the coefficient of convective heat exchange in relation to the used fluid and the adopted configuration. The liquid metal has high values of h, about 10^4, while the air, as it was obvious to expect, presents values of the convective coefficient two orders of magnitude lower compared with the first. The diathermic oil, used for the configuration 4, instead, determines a value of h one order of magnitude lower than the liquid metal. The heat flux exchanged through the contact solid/fluid, predictably, decreases with increasing of the wetted area by the fluid. Therefore, the configurations with an increased number of fins have a lower heat flux. It is interesting to observe that configuration 5 is characterized by an average bulk temperature of the fluid lower than all other configurations.

The comparison with the empirical correlations is diversified in relation to the heat transfer fluid adopted.

The evaluation of the gap between the obtained solution with the CFD analysis and the one obtained with the empirical relationships was assessed by the percentage error with the following equation:

$$|\varepsilon|\% = \frac{h_{\mathrm{calculated}} - h_{\mathrm{empirical}}}{h_{\mathrm{calculated}}} \times 100 \quad (15)$$

Table 6 shows the percentage errors for the simulations implemented with liquid metal and correlations (9)–(12). The errors are generally high for all configurations despite

Table 5 Calculus of the convective coefficients

	T_w (°C)	T_b (°C)	q_w (W m^{-2})	h (Wm^{-2} K^{-1})
1 (NaK)	574.84	576.55	33,160	19,391
2 (NaK)	575.36	577.25	24,357	12,887
3 (NaK)	574.79	575.85	21,795	20,561
4 (NaK)	574.95	576.57	17,738	10,949
4 (Air)	460.92	554.09	13,040	139
4 (Oil)	384.76	393.34	10,579	1232
5 (NaK)	572.32	574.26	242,46	12,497

Table 6 Percentage errors for liquid metals

	Equation (9)	Equation (10)	Equation (11)	Equation (12)
1 (NaK)	49.90	63.23	63.55	67.81
2 (NaK)	2.48	26.07	22.58	31.17
3 (NaK)	31.61	50.81	47.96	53.72
4 (NaK)	56.28	40.62s	35.38	7.96
5s (NaK)	22.27	42.94	43.44	50.05
5c (NaK)	0.13	27.75	25.04	33.40

Table 7 Percentage errors for air

	Equation (7)	Equation (8)
4 (Air 728 °C)	49.95	24.17
4 (Air 478 °C)	39.8	5.77

Table 8 Percentage errors for diathermic oil

	Equation (7)	Equation (8)
4 (oil)	51.21	58.29

Table 9 Characteristic temperature for the different fluids

	T_i (°C)	T_u (°C)	ΔT (°C)	T_b (°C)
1 (NaK)	582.0	572.2	9.8	576.55
2 (NaK)	582.0	572.3	9.7	577.25
3 (NaK)	582.0	572.3	9.7	575.85
4 (NaK)	582.0	572.2	9.8	576.57
4 (Air)	728.0	493.0	235.0	559.04
4 (Oil)	394.4	392.4	2.0	393.34
5 (NaK)	582.0	572.4	9.6	574.26

the orders of magnitude of the convective coefficients being similar. Moreover, it can be seen that errors for a given correlation are different at variation of the configuration. Lyon's equation [20], Eq. (9), better approximates the CFD results with high percentage error only for configurations 1 and 4. Configuration 1 shows greater average errors than the other configurations.

The comparison of results obtained by CFD simulations with air, only for configuration 4, and those provided by the correlations (7) and (8), are quoted in Table 7.

Roger and Mayhev's correlation [14] has greater error than Xin and Ebadian's correlation [15]. These correlations, as already said, are the only ones that directly take into account the curvature of the heat exchanger.

The application of these correlations to liquid metals led to significant errors, showing that they are not applicable to these types of fluids.

In Table 8, finally, there is the comparison of the CFD simulations and the predictions of the empirical correlations (7) and (8) for the diathermic oil.

Roger and Mayhev's equation best approximates the data provided by the simulation while Xin and Ebadian's correlation has almost 60 % errors. The two correlations provide better results using air as the heat transfer fluid. A further comparison was attempted with the correlations pertaining to liquid metals with poor results.

In conclusion, despite the errors found being meaningful, the convective heat transfer coefficients have comparable orders of magnitude.

The cause of the differences between experimental data and computer simulations has to be sought in conditions under which the tests are performed. Indeed, the geometry used for the determination of the empirical correlations is different from that used in CFD simulations. On the other hand, in some problems of thermo-fluid dynamics, variance of about 100 % should not be considered impossible. Sure enough, simulations on liquid metals have to be considered satisfactory. Further research could be aimed at the turbulent Prandtl number's definition for geometries similar to the one under investigation in experimental trials. A new CFD study based on this value could be set up with testing of the results with the correlations described above.

Energetic consideration

Studies conducted up to this point are preliminary to the choice of the most efficient configuration of the component adapted to transmit the power from the hot fluid to the surface of contact with the Stirling engine. An overall quantitative comparison will be made on data obtained from CFD simulations.

The operating temperatures of the fluid are of crucial importance for the energy efficiency definition of the system but also to determine the design parameters and the devices to operate for a possible creation of the model. Table 9 shows the temperature of the fluid in the input (T_i) and outlet section (T_u), and the difference between these two values. Furthermore, the average temperature is viewable on the entire volume, previously used for the evaluation of the convective heat exchange coefficient. Maintaining constant the inlet temperature for all

simulations with liquid metal, different temperature in the output section at variation of the exchanger geometry can be pointed out. This parameter is an indication of how much the fluid in the flow inside the heat exchanger cooled. Greater temperature differences (ΔT) cause a better transferring of power from the fluid to the Stirling head. This parameter remains approximately constant for all configurations with liquid metal. Clearly, changing the heat transfer fluid, changes the meaning of the temperature difference between the inlet and outlet because it changes the possibility of the fluid transferring power to the surface. For this reason, air undergoes a sharp drop in temperature but this does not require the greater transfer of power than that calculated with the liquid metal. With flow rate input greater, and consequent increase in the velocity, and at equal power exchanged, lower gradients would be obtained. This option was discarded during the setup process in Fluent because of the additional complications that would be introduced with increased turbulence. Oil instead is an excellent heat transfer fluid, almost comparable to the liquid metals but with the disadvantage of having too low a boiling temperature.

Table 10 summarizes the results produced by CFD simulations plotting the temperatures on the contact surface with the Stirling engine head. These are the calculated average temperature (T_{sc}) and the temperature (T_{sa}) selected during the setup phase to be able to operate under conditions closer to the nominal values of the Stirling engine (565 °C).

Although a precise congruence between the calculated data and the expected data is not obtained, total deviation of 3 °C at the peak can be considered acceptable. This convergence was not tested only on the air because of its low thermal capacity.

In the same Table the difference is shown between the inlet temperature of the fluid and the Stirling contact zone temperature, representative of the heat exchange efficiency. If this temperature difference, ideally, might be zero, one would obtain a heat exchanger with unit efficiency.

$$\Delta T_c = T_i - T_{sc} \tag{16}$$

Table 10 Characteristic temperature for the contact surface

	T_{sa} (°C)	T_{sc} (°C)	ΔT_c (°C)
1 (NaK)	558	557.8	24.2
2 (NaK)	558	560.4	21.6
3 (NaK)	560	559.9	22.1
4 (NaK)	561	559.3	22.7
4 (Air)	448	438.0	290.0
4 (Oil)	371	370.7	23.7
5 (NaK)	553	552.0	30.0

Table 11 Thermal, electric and pumping power

	P_{cal} (W)	P_{el} (W)	P_{pom} (W)
1 (NaK)	4519	1063	0.49
2 (NaK	4473	1073	0.64
3 (NaK)	4473	1072	0.53
4 (NaK)	4519	1071	0.66
4 (Air)	3367	721	39.40
4 (oil)	2567	530	0.62
5 (NaK)	4427	1051	0.65

This difference substantially decreases passing from configuration 1 to those with fins, obtaining the minimum value in the case of two fins. The transition from geometry with two fins to a geometry with five fins resulted in less turbulent flows causing a reduction in the energy transport. This result is more evident for configuration 5 with transverse fins. The results of CFD simulations with air showed ΔT_c values significantly higher than the other fluids.

The CFD analysis allowed the estimation of the pressure loss inside the heat exchanger providing the pressure difference between the input section and the output section.

Table 11 shows the total heat transfer rate absorbed by the engine, the electric power and the pumping power.

As expected, the pumping power for the air is considerably higher compared to the other fluids. The transferred power by the heat transfer fluid, in the same way, is comparable between the flows with liquid metal, while it is lower for air and oil. This trend is also followed by the electrical power output from the Stirling engine.

The evaluation of the heat exchanger performance is obtained through the ratio between the real power transferred from the fluid and the maximum power that could be yielded in ideal conditions Eq. (17). The latter is made up of the power which the Stirling engine would absorb if the contact temperature between the engine and the heat exchanger were equal to the inlet temperature of the fluid. The maximum power is obtainable from Eq. (2) by inserting the inlet temperature of the fluid.

$$\eta = \frac{P_{cal}}{P_{max}} \tag{17}$$

Table 12 Efficiency with the different configurations

	η
1 (NaK)	0.95
2 (NaK	0.91
3 (NaK)	0.94
4 (NaK)	0.95
4 (Air)	0.41
4 (Oil)	0.89
5 (NaK)	0.93

The following table (Table 12) shows the efficiency values for the different configurations. The maximum value is obtained for configuration 1 and 4, with the liquid metal.

The simulation with air results in a very low efficiency compared to the other cases studied. The use of thermal oil, in contrast, leads to lower values than the liquid metals, but comparable with the latter.

Conclusions

In this work the sizing of a heat exchange, which is the hot source for the head of a Free Piston Stirling Engine, beta configuration, was carried out. The external geometry of the heat exchanger proposed is made up of a toroidal body that wraps itself around the circular contact surface with the engine. This is the only area dedicated to the power transfer from the heat exchanger to the head. Five different configurations for the internal geometry of the exchanger were analysed. The first is fundamental for successive configurations. An increasing number of longitudinal fins were inserted with respect to the fluid flow from the second to the fourth configurations. The fifth and final configuration has twelve transverse fins to the flow.

The thermal performance of the heat exchanger is strongly influenced by the type of heat transfer fluid used. In this connection, a comparison was made of three fluids: air, thermal oil and liquid metal.

The thermo-fluid study of heat exchanger was conducted through fluid dynamic simulations on the computer (CFD).

The results obtained from CFD showed a fairly good agreement with the results obtained from empirical correlations sought in the scientific literature, considered to be applicable to the present case. Specifically, although the percentage deviation calculated is high, the controlled variables have the same order of magnitude. A necessary study should be devoted to the research of the turbulent Prandtl number for the flows with eutectic alloy of sodium and potassium, through empirical testing. This parameter is of fundamental importance for the liquid metals in the case of turbulent regime. Despite the uncertainty of the results achieved, conclusions can be inferred in relation to the configurations and fluids used.

Configurations that use the NaK as heat transfer fluid involve energy yields greater than configurations that use other fluids, with values comprised between 91 and 95 %. With this fluid, characterized by excellent thermophysical properties, the Stirling engine always works in nominal conditions regardless of the configuration used and, therefore, it becomes unnecessary to resort to fins in the exchanger.

The use of thermal oil as heat transfer fluid, because of its low boiling temperature, entails, indeed, electric-produced power in the order of 60 % of nominal power.

The performance of these systems could greatly improve with the use of next-generation fluids (nanofluids) that are still being tested.

References

1. Bakos, G.C., Antoniades, Ch.: Techno-economic appraisal of a dish/stirling solar power plant in Greece based on an innovative solar concentrator formed by elastic film. Renew. Energy **60**, 446–453 (2013)
2. Cucumo, S., Faini, G., Laino, L., Marino, M., Pastorelli, E.: Analisi e sperimentazione di un assorbitore per un sistema dish-stirling di piccola taglia, 66° Congresso Nazionale ATI, Rende (Cosenza)(2011)
3. Dicorato, M., Forte, G., Pugliese, P., Trovato, M., Pulito, V.: Analisi delle potenzialità di un sistema solare termodinamico per la produzione di energia elettrica e termica, Atti del Congresso Nazionale AEIT 2009, 28-30 Settembre. Catania, Italia (2009)
4. Dicorato, M., Forte, G., Pisani, M., De Tuglie, M.: One-axis tracking optimization of concentrating solar power for electricity production. Proceedings of UPEC 2010, 45th International Universities' Power Engineering Conference, Cardiff (2010)
5. Pacio, J., Wetzel, Th: Assessment of liquid metal technology status and research paths for their use as efficient heat transfer fluids in solar central receiver systems. Sol. Energy **93**, 11–22 (2013)
6. Srinivasan, S., Nandapurkar, S., Holland, F.A.: Friction factors for coils. Trans. Instit. Chem. Eng. **48**, T156–T161 (1970)
7. Ito, H.: Friction factors for turbulent flow in curved pipes. J. Basic Eng. **81**, 123–134 (1959)
8. Di Liberto, M., Ciofalo, M.: A study of turbulent heat transfer in curved pipes by numerical simulation. Int. J. Heat Mass Transf. **59**, 112–125 (2013)
9. Anderson Jr, J.D.: Computational fluid dynamics. The basics with applications. McGraw-Hill, New York (1995)
10. Blazek, J.: Computational fluid dynamics: principles and application. Elsevier, Amsterdan (2008)
11. ANSYS: ANSYS Fluent Theory guide, Release 14.7. ANSYS Inc., Canonsburg (2011)
12. ANSYS: ANSYS Fluent User's guide, Release 14.7. ANSYS Inc., Canonsburg (2011)
13. ANSYS: ANSYS Fluent V2F turbulence model manual, Release 14.7. ANSYS Inc., Canonsburg (2011)
14. Rogers, G.F.C., Mayhew, Y.R.: Heat transfer and pressure loss in helically coiled tubes with turbulent flow. Int. J. Heat Mass Transf. **7**, 1207–1216 (1964)
15. Xin, R.C., Ebadian, M.A.: The effects of Prandtl numbers on local and average convective heat transfer characteristics in helical pipes. J. Heat Transfer **119**, 467–473 (1997)

16. Cheng, X., Tak, N.: CFD analysis of thermal–hydraulic behaviour of heavy liquid metals in sub-channels. Nucl Eng. Design, **236**, 1874–1885 (2006)
17. Aoki, S.: A consideration on the heat transfer in liquid metal. Bull. Tokyo Inst. Technol. **54**, 63–73 (1963)
18. Dwyer, O.E.: Recent developments in liquid metal heat transfer. Atom. Energy Rev. **4**(1), 3–92 (1966)
19. Reynolds, A.J.: The prediction of turbulent Prandtl and Schmidt numbers. Int. J. Heat Mass Transf. **18**, 1055–1069 (1975)
20. Cheng, X., Tak, N.: Investigation on turbulent heat transfer to lead–bismuth eutectic flows in circular tubes for nuclear applications. Nucl. Eng. Design, **236**, 385–393 (2006)
21. Lyon, R.N.: Liquid metal heat transfer coefficients. Chem. Eng. Prog. **47**, 75–79 (1951)
22. Martinelli, R.C.: Heat transfer to molten metals. ASME Trans. **69**, 47–59 (1947)
23. Skupinski, E., Tortel, J., Vautrey, L.: Tetermination des coefficients de convection D'un Alliage sodium–potassium Dans un Tube circulaire. Int. J. Heat Mass Transf. **8**, 937–951 (1965)
24. Sleicher, C.A., Awad, A.S., Notter, R.H.: Temperature and Eddy diffusivity profiles in NaK. Int. J. Heat Mass Transf. **16**, 1565–1575 (1973)
25. Kirillov, P.L., Ushakov, P.A.: Heat transfer to liquid metals: specific features, methods of investigation, and main relationships. Therm. Eng. **48**(1), 50–59 (2001)
26. Stromquist, W.K.: Effect of wetting on heat transfer characteristics of liquid metals, ORO-93. University of Tennessee, Knoxville (1953)